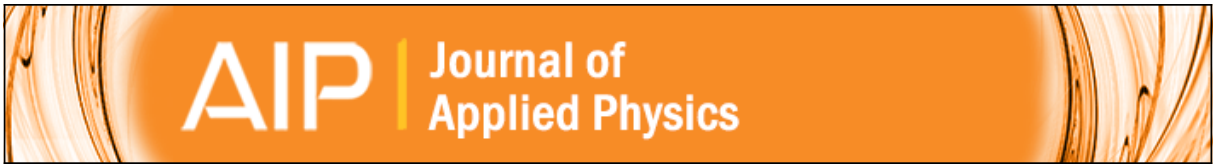

Exponential critical state model applied to ac susceptibility data for the superconductor YBa2Cu3O7

F. M. AraújoMoreira, W. A. Ortiz, and O. F. de Lima

Citation: Journal of Applied Physics **80**, 3390 (1996); doi: 10.1063/1.363204

View online: http://dx.doi.org/10.1063/1.363204

View Table of Contents: http://scitation.aip.org/content/aip/journal/jap/80/6?ver=pdfcov

Published by the AIP Publishing

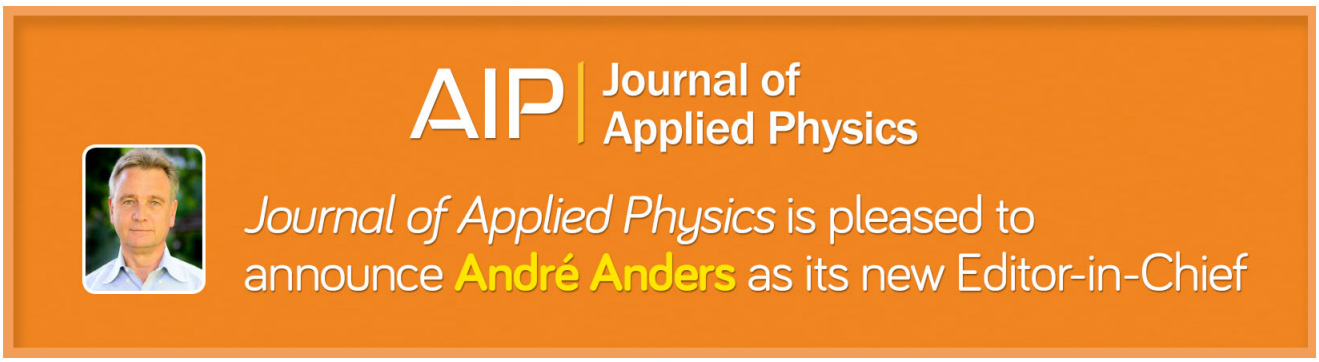

Exponential critical state model applied to ac susceptibility data for the superconductor $YBa_2Cu_3O_{7-\delta}$

F. M. Araújo-Moreira[a] and W. A. Ortiz
Departamento de Física, Universidade Federal de São Carlos, C.P. 676 13565-905, São Carlos, SP, Brazil

O. F. de Lima[b]
Instituto de Física ''Gleb Wataghin,'' Unicamp 13083-970, Campinas, SP, Brazil

(Received 25 September 1995; accepted for publication 31 May 1996)

We derive new expressions for the average magnetization loops, $M(H)$, based on the exponential critical state model. The components χ' and χ'' of the complex susceptibility are calculated and an algorithm to fit ac susceptibility data is discussed. This algorithm is employed to study the intergranular response $\chi'(H_m)$ and $\chi''(H_m)$ measured for two samples of $YBa_2Cu_3O_{7-\delta}$ as a function of the ac field amplitude H_m. One sample is a porous sintered cylinder and the other is a very dense melt-textured bar. In both cases good fits of the calculated components χ' and χ'' are obtained using an algorithm that involves two free parameters, the full penetration field, H_p, and the sample quality factor, p. An interesting result for the melt-textured sample is the observation of a step in $\chi'(H_m)$ curves at very low H_m, possibly associated with grain clustering. © *1996 American Institute of Physics.* [S0021-8979(96)05917-8]

I. INTRODUCTION

Persistent shielding currents circulating on superconductors can be detected by magnetization and susceptibility measurements. dc or ac susceptibility may be measured using direct or alternating magnetic fields.[1] These types of measurements have been widely used to accurately determine the critical temperature (T_c) of conventional metallic superconductors and, in recent years, to measure the magnetic transition of high-T_c oxide superconductors.[2] In these latter materials, detailed ac susceptibility measurements as a function of temperature and ac field amplitude, H_m, typically show two drops in the real component, χ', and two corresponding peaks in the imaginary component, χ'', when H_m exceeds some threshold value which depends on sample quality.[3,4] This suggests a granular behavior such that superconducting regions or grains are coupled through weak links or Josephson-type junctions, reflecting low values of transport critical current densities,[4,5] J_c, typically of the order of 10^3 A/cm^2. An extremely short coherence length, which is characteristic of high-T_c oxide superconductors, combined with oxygen deficiency at grain and twin boundaries, seem to be the main sources of this weak-link behavior. However, it becomes clear that low critical currents are not intrinsic because very high J_c values have been obtained in single crystals and films of these materials.[6,7] On the other hand, ac susceptibility measurements as a function of H_m and in a fixed low temperature, typically show two plateaus and two peaks in the real and imaginary parts, respectively.[8,9] The first plateau at lower H_m values is associated with total magnetic shielding of the sample. The second plateau is associated with shielding of the grains only, allowing magnetic field along the grain boundaries, generally a very poor superconducting material. By increasing H_m above the second plateau, exceeding the bulk lower critical field H_{c1}, flux penetrates into the grains.

Susceptibility data for polycrystalline samples are complicated to analyze quantitatively. The fraction of intergranular material, the shape, size, and demagnetization factors of the whole sample and grains, the anisotropy of current inside and between grains, the flux pinning properties of granular and intergranular materials, the volume distribution of superconducting parameters, and the coupling properties between grains, are the main factors that influence susceptibility data.

In this paper we apply an exponential critical state model to analyze some ac susceptibility data, obtained for two samples of the high-T_c superconductor $YBa_2Cu_3O_{7-\delta}$. A good quantitative agreement is found, based on simple phenomenological ideas. Following, we review the main points of the theory in Sec. II, present some computer simulations in Sec. III, a discussion of the experimental and fitted results in Sec. IV, and the conclusions in Sec. V.

II. EXPONENTIAL CRITICAL STATE MODEL

The concept of critical state model was introduced by Bean[10,11] and London[12] in a successful effort to derive magnetic properties of hard type-II superconductors. Different critical state models,[8,13–15] which assume that supercurrents flow inside the sample with a critical density $J_c(H_i)$, where H_i is the internal magnetic field, have been used to study the response of type-II superconductors to an external field H.[16–18] In particular Chen *et al.*[17] have shown that the exponential law, $J_c(H_i,T)=J_c(T)\exp(-H_i/H_0)$, originally introduced by Fietz *et al.*,[14] is very useful to interpret ac susceptibility data of high-T_c superconductors. Following, we show the main steps of the calculation which is allowed to express the complex susceptibility, $\chi=\chi'+i\chi''$, in terms of the exponential critical state model.

Cooling a type-II superconductor sample below its critical temperature a volume fraction of the sample becomes

[a]Present address: Center for Superconductivity Research, Department of Physics, University of Maryland, 20742 College Park, Maryland.
[b]Electronic mail: delima@ifi.unicamp.br

 0021-8979/96/80(6)/3390/6/$10.00

superconducting so that χ' decreases with decreasing temperature. When $\chi' = -1$ (SI units) the sample is completely shielded by supercurrents circulating on its surface layer. To interpret ac susceptibility data of high-T_c oxide superconductors, we use a critical state model where the sample is considered to consist of superconducting grains, embedded in a normal or weakly coupled superconducting matrix. Thus, we can write the complex susceptibility in the form:

$$\chi = \chi_g f_g + (1 - f_g)\chi_m, \tag{1}$$

where χ_g and f_g are the complex susceptibility and the effective volume fraction of grains, respectively, which can be evaluated directly from the experimental data for χ' as will be subsequently discussed. χ_m is the complex susceptibililty for the remaining volume after removing the grain cores,[19] or simply labeled as the matrix. Assuming an ac field amplitude lower than H_{c1} of the grains for the temperature considered, we can state that $\chi'_g = -1$ and $\chi''_g = 0$. Therefore, the real and imaginary components of χ in Eq. (1) can be written as

$$\chi' = -f_g + (1 - f_g)\chi'_m, \tag{2a}$$

$$\chi'' = (1 - f_g)\chi''_m. \tag{2b}$$

The values of χ'_m and χ''_m are defined as the first components of the complex harmonic susceptibility[20] that come from the Fourier analysis of the time-dependent magnetization, as follows:

$$\chi'_m = \frac{2}{H_m \pi}\int_0^{\pi} M(\theta)\cos(\theta)\, d\theta, \tag{3a}$$

$$\chi''_m = \frac{2}{H_m \pi}\int_0^{\pi} M(\theta)\sin(\theta)\, d\theta, \tag{3b}$$

where H_m is the amplitude of the ac magnetic field $H(t) = H_m \cos(\theta)$, with $\theta = \omega t$, and $\omega = 2\pi f$ being the fundamental frequency of the applied field *H(t).*

Equations (3a) and (3b) are evaluated numerically and the calculated values are inserted in Eqs. (2a) and (2b) in order to obtain χ' and χ''. The time-dependent magnetization, $M(\theta)$, which is the same as $M(H)$, can be calculated by averaging the local magnetization over the sample cross-sectional area. For the case of an infinite column having circular or square cross section, of radius a or side $2a$, it can be readily shown that the averaged magnetization becomes

$$M = \frac{2}{a^2}\int_0^a x' M_i(x')\, dx', \tag{4}$$

where $M_i(x') = [H_i(x') - H]$ is the local magnetization at point x', being directly related to a supercurrent closed path that is established at a distance $(a - x')$ from the sample surface. Chen *et al.*[17] have presented the following very general form, valid for infinite columnar samples with the cross section so that the supercurrent closed path length is given by $4(cx' + b - a)$ and the cross section area by $2ca^2 + 4(b-a)a$:

$$M = \left[\frac{ca^2}{2} + (b-a)a\right]^{-1}\int_0^a (cx' + b - a)M_i(x')\, dx', \tag{5}$$

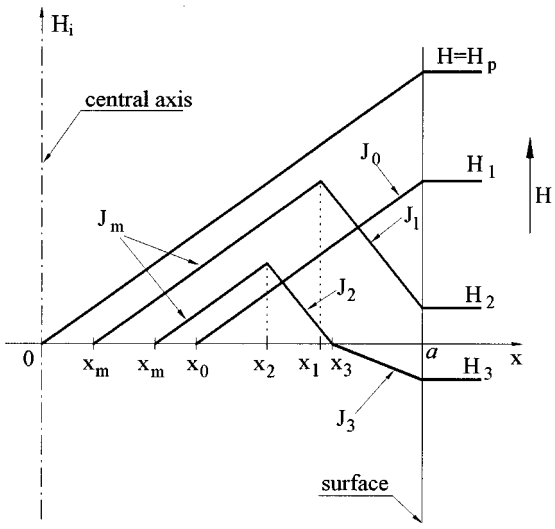

FIG. 1. Schematic view of typical profiles of the magnetic field inside the sample, as the external field varies from zero to H_1, H_p, H_2 and H_3. The supercurrent densities J_0, J_m, J_1, J_2, and J_3 are associated with the field gradients in different regions (or layers) whose boundaries are located at points $x = 0, x_0, x_1, x_2, x_3, a$. The center and surface are located at $x = 0$ and $x = a$, respectively.

where a and b are relevant linear dimensions of the cross-section $(a < b)$, and c is a coefficient appropriate to each particular geometry. For instance, when $c = 2$, Eq. (5) describes a rectangular cross section having sides $2a$ and $2b$. When $a = b$, Eq. (5) simplifies to Eq. (4).

In order to calculate $M_i(x')$, one has to consider all possibilities for the internal field profile, $H_i(x)$, generated during the magnetization loop, which is caused by the alternating field *H*. Figure 1 is a qualitative representation of four typical profiles of $H_i(x)$ occurring when the applied field H varies from 0 up to H_m (generating the initial magnetization curve) and down to $-H_m$ (generating the reverse magnetization curve). For simplicity, the lower critical field H_{c1} is assumed to be negligible, meaning that the magnetization process is totally determined by the critical state model.

When H increases from zero (e.g., $H = H_1$ in Fig. 1) a supercurrent layer is established adjacent to the surface, shielding the volume surrounded by this layer against the applied field H. In this layer, whose inner boundary is located at $x = x_0$, the induced supercurrent is negative and denoted by $J_0(x)$. This boundary moves towards the center of the sample when H increases, reaching eventually the center $(x_0 = 0)$ for $H = H_p$, the full penetration field. For $H > H_p$ the supercurrent remains $J_0(x)$ over the entire cross section. A new outer layer, having positive supercurrent value $J_1(x)$, is established when H decreases from H_m (e.g., $H = H_2$ in Fig. 1). This outer layer is bounded by the sample surface and intersects the previous inner layer at $x = x_1$. The critical current density $J_m(x)$ associated with the inner layer is established at $H = H_m$ and its inner boundary is located at $x = x_m$. By decreasing H the boundary at x_1 is pushed towards the center of the sample, but the typical profile remains the same of $H = H_2$, until $H = 0$. When H changes its sign, $H_i(x)$ also reverses its sign in a new outer layer, start-

ing at the sample surface and ending at the intersection point $x=x_3$ (e.g., $H=H_3$ in Fig. 1). Thus, the supercurrents are now separated in three regions (or layers) $J_m(x)$, $J_2(x)$, $J_3(x)$, with their inner boundaries at x_m, x_2, x_3, respectively.

For an isothermal situation the exponential critical state model predicts

$$J_c(H_i)=k\ \exp\left(-\frac{|H_i|}{H_0}\right), \tag{6}$$

where k and H_0 are positive constants.

Using Ampere's law we have:

$$\frac{dH_i}{dx}=-J_c(H_i)=-k\ \exp\left(-\frac{|H_i|}{H_0}\right). \tag{7}$$

By integration of Eq. (7) the following general expression is obtained:

$$J_n(x)=-\mathrm{sgn}\left(\frac{dH_i}{dx}\right)\frac{H_0}{(x+c_n)}, \tag{8}$$

where sgn(x) is the sign-function, and the subscript n identifies the layer inside the sample (see Fig. 1) which carries the supercurrent density $J_n(x)$, c_n being an integration constant to be determined from boundary conditions involving adjacent layers.[17]

The local field, $H_i(x)$, can be obtained by integration of the supercurrent density, *J(x)*, that forms closed paths distributed over the sample cross section:

$$H_i(x)=H+\int_x^a J(x')dx'. \tag{9}$$

Using $M_i(x)=H_i(x)-H$ the local magnetization then becomes

$$M_i(x)=\int_x^a J(x')dx', \tag{10}$$

where $J(x')$ is generally divided into several contributions as shown in Fig. 1.

There is an initial $M(H)$ curve that occurs only during the first half cycle of H $(0\rightarrow H_m)$, beginning with the sample in the virgin magnetic state. After this initial $M(H)$ curve follow the $M(H)$ reverse curves, that correspond to the cyclic response of the sample to the alternating field H, $(H_m\leftrightarrow -H_m)$.

A set of equations for all possibilities of $M(H)$ appears in Ref. 17. However, we found that two of these equations are wrong, namely Eqs. (21d) and (21e), corresponding to terms M_6 and M_7. For instance, these expressions diverge when $H\rightarrow 0$. We then derived the following new expressions which were employed to analyze our data:

$$M_6=\frac{H_o}{G}\left[-\frac{H}{H_o}-\ln(F_6)\right]\left[\frac{cx_3^2}{2}+(b-a)x_3\frac{cx_2^2}{2}-(b-a)x_2\right]$$
$$+\frac{H_o^2}{kG}\left[\frac{cH_o}{k}+cx_3+b-a\right][1+F_7\ \ln(F_7)-F_7]$$
$$-\frac{caH_o^2}{2pkG}\left[\frac{1}{2}+F_7^2\left(\ln(F_7)-\frac{1}{2}\right)\right], \tag{11}$$

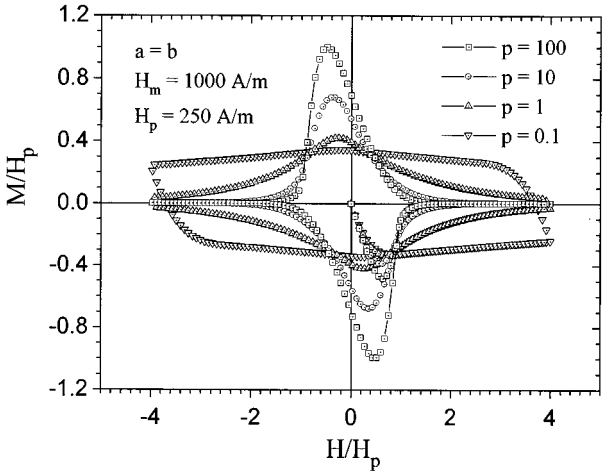

FIG. 2. Plot simulations of $M(H)$ for a columnar sample of circular or squared cross section ($a=b$), for various values of the fitting parameter p. When p increases, the width of the hysteresis loop decreases.

$$M_7=-\frac{H}{G}\left[\frac{ca^2}{2}+(b-a)a\frac{cx_3^2}{2}-(b-a)x_3\right]$$
$$-\frac{H_o^2ca}{2pkG}\left[\frac{1}{E^2}\left(-\frac{H}{H_o}-\frac{1}{2}\right)+2\left(p-\frac{1}{E}\right)\right.$$
$$\left.\times\left(F_6-F_6\ \ln(F_6)-\frac{1}{E}\frac{H}{H_o}-\frac{1}{E}\right)\right]$$
$$+\frac{H_o^2ca}{2pkG}F_6^2\left[\ln(F_6)-\frac{1}{2}\right]$$
$$+\frac{H_o^2(b-a)}{kG}\left[F_6\ \ln(F_6)-F_6+\frac{1}{E}\frac{H}{H_o}+\frac{1}{E}\right], \tag{12}$$

where F_6, F_7, G, E, and $p=ka/H_0$ are defined in Ref. 17.

The corresponding expressions for the local magnetization that goes into Eq. (5) are

$$M_i^{(6)}(x)=\int_x^{x_3}J_2(x')dx'+\int_{x_3}^a J_3(x')dx'$$
$$=H_o\left[\ln\left(1+\frac{kx_3}{H_o}-\frac{kx}{H_o}\right)+\ln\left(\frac{1}{E}\right)-\ln(F_6)\right] \tag{13}$$

$$M_i^{(7)}(x)=\int_x^a J_3(x')dx'$$
$$=H_o\left[\ln\left(\frac{1}{E}\right)-\ln\left(\frac{1}{E}-\frac{ka}{H_o}+\frac{kx}{H_o}\right)\right]. \tag{14}$$

III. COMPUTER SIMULATIONS

Three computer programs were written in language *C* that are allowed to simulate $M(H)$ curves (program 1), $\chi(H_m)$ curves (program 2), and to plot them (program 3). Using programs 1 and 2 in a self-consistent way the best fit of ac susceptibility data can be obtained quickly, as will be discussed in Sec. IV.

Figures 2 and 3 show simple simulations of $M(H)$ and $\chi(H_m)$ curves, for a columnar sample having circular or

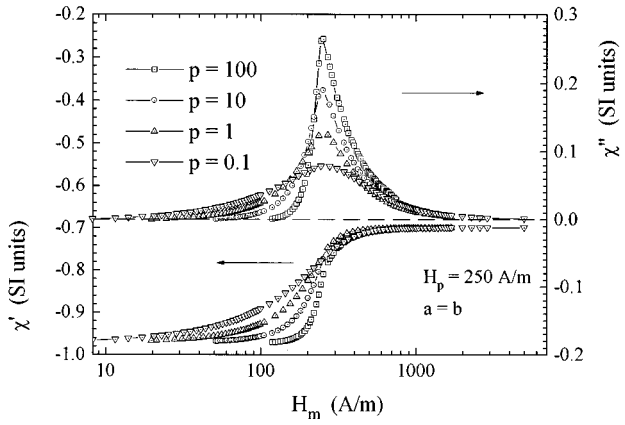

FIG. 3. Plot simulations of $\chi'(H_m)$ and $\chi''(H_m)$ for a columnar sample of circular or squared cross section ($a = b$), for various values of the fitting parameter p. When p increases, the width of the superconducting transition sharpens, as seen in both components $\chi'(H_m)$ and $\chi''(H_m)$.

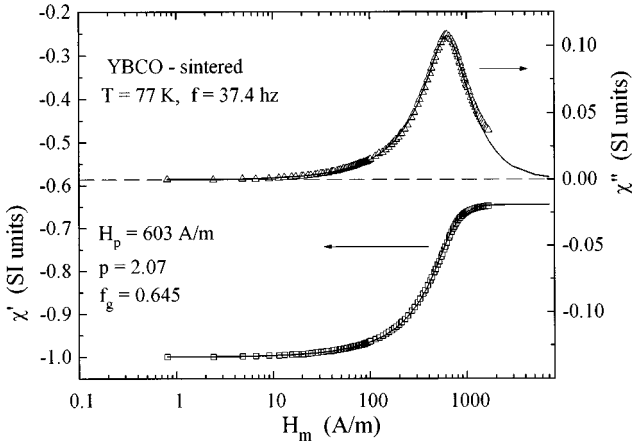

FIG. 4. Data points for both components of the ac susceptibility as a function of the magnetic field amplitude for the YBCO-sintered sample. In the field interval shown only the intergranular material has been penetrated by the field. Solid lines represent the exponential critical state model fit to the data.

squared cross section ($a = b$ and $c = 2$). A full penetration field $H_p = 250$ A/m and a maximum ac field amplitude $H_m = 1000$ A/m were used to generate Fig. 2. Both figures illustrate the effect of changing the parameter p between 0.1 and 100. The superconducting transition width, given roughly by the hysteresis loop width (Fig. 2) or by the peak width of $\chi''(H_m)$ (Fig. 3), is narrowed when p increases. From the definition of the full penetration field,[17] $H_p = H_0 \ln(1+p)$, it can be readily shown that

$$\frac{J_c(0)}{J_c(H_p)} = 1 + p, \tag{15}$$

where $J_c(H_p)$ and $J_c(0)$ are the critical supercurrent densities, respectively, at the surface ($x = a$) and at the center ($x = 0$) of the sample, when $H = H_p$. This means that for higher p values the field dependence of $J_c(H_i)$ is stronger and the gradient of $H_i(x)$ is higher. Therefore, parameter p can be correlated with the spatial uniformity of $J(x)$ inside the sample[21] and could be eventually used to label the sample quality with respect to its microstructure.

IV. EXPERIMENTAL RESULTS

We have applied the critical state model described in this paper to analyze ac susceptibility data for two samples of the high-T_c cuprate $YBa_2Cu_3O_{7-\delta}$ (YBCO). One sample was sintered using the solid diffusion method, starting from a stoichiometric mixture of Y_2O_3, CuO, and Ba_2CO_3. This sample, labeled as YBCO-sintered, has a cylindrical shape with a radius $a = 1.39$ mm and height 6.0 mm. The microstructure characterization, using scanning electron microscopy in a fractured cross section, revealed a large amount of porosity and grain sizes below 10 μm. Measurements of χ' vs T curves at zero field showed a relatively broad transition with $T_c \approx 92.0$ K at the onset point.

The second sample, labeled as YBCO-MTG, was obtained by the partial-meltgrowth method.[22] It has grains well aligned in the c axis direction, checked by an x-ray rocking curve for the (005) peak that reveals an angular spread around 0.5°. The sample is a column having an approximately rectangular cross section, with sides $2a = 1.2$ mm and $2b = 2.6$ mm. A careful analysis of the microstructure was done using optical microscopy and scanning electron microscopy. A dense array of well aligned platelike grains, with typical cross section around 400×80 μm^2, can be observed with some impurity traces of Y_2BaCuO_5 and $BaCuO_2$, located mainly along the grain boundaries. For the YBCO-MTG sample, the χ' vs T curve at zero dc field has exhibited a sharp transition, with $T_c \approx 91.0$ K at the onset point.

Figures 4 and 5 show ac susceptibility versus H_m data points, respectively for the sintered and MTG samples, taken

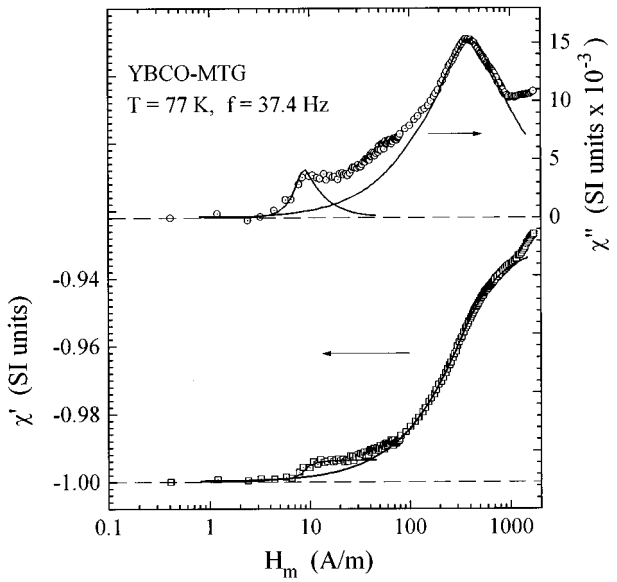

FIG. 5. Data points for both components of the ac susceptibility as a function of the magnetic field amplitude for the YBCO-MTG sample. Two plateaus in χ' and the associated two maxima in χ'' can be seen at $H_m \approx 8.5$ A/m and $H_m \approx 334$ A/m. Solid lines represent the exponential critical state model fit to the data.

at liquid nitrogen temperature (77 K) and using a frequency of 37.4 Hz for the excitation field whose amplitude varied between 1 and 1760 A/m. The MTG data were obtained with the ac magnetic field applied nearly parallel to the grains **c**-axis. In Figs. 4 and 5 we also see solid lines that go along with the experimental points, representing the best fits of the exponential critical state model. Notice that these data correspond only to the matrix response caused by the field penetration through weak links (grain boundaries, pores, normal precipitates) and the London surface layer of the grains.[19] The process of field penetration produces χ' curves with a typical ''S'' shape, showing a plateau that separates the response due to intragrain currents at higher fields. The corresponding χ'' curves exhibit a maximum in the same field region of the steepest part of χ'. Figure 5 shows clearly two plateaus in χ' and the associated two maxima in χ'', which are located around $H_m = 8.5$ A/m ($\sim$0.107 Oe) and 334 A/m ($\sim$4.203 Oe).

Combining Eqs. (2a)–(2b), (3a)–(3b), and the equations for $M(H)$, we obtain an algorithm that contains only H_p and p as free parameters. The effective volume fraction of grains appearing in Eqs. (2a) and (2b) is evaluated as $f_g = -\chi'_g$ where χ'_g is the calibrated experimental value at the first plateau. Thus, we assume that only the grains remain unpenetrated by the magnetic field H when this plateau is reached. For the MTG sample (Fig. 5) the occurrence of two plateaus prevents a simple and unequivocal determination of χ'_g. Possibly the first plateau at lower field is an indication of grain clustering,[19] while the second plateau at higher field corresponds to the tightly joined grains inside the clusters. Hence, a multilevel granular structure would be present, raising some concern about the application of critical state models that assume an uniform current distribution across the sample.

In order to fit the model to our data a recursive approach for the numerical calculation is employed, by playing with the two fitting parameters H_p and p. The final calculated curves for χ' and χ'', which are represented by the solid lines in Figs. 4 and 5, are found quickly in a very effective way. It is important to stress that both components, χ' and χ'', are tied to each other as shown by Eqs. (3a)–(3b). This means that when the best values for H_p and p are found, both components become fitted simultaneously.

The result of the fit shown in Fig. 4 for the YBCO-sintered sample with $f_g = 0.645$ is excellent, producing $H_p = 603$ A/m ($\sim$7.6 Oe) and $p = 2.07$. An overall volume average of the critical current density is $\langle J_c \rangle = H_p/a \approx 44$ A/cm^2. These values are comparable to previous results reported by Sanchez *et al.*[23] for a sintered YBCO sample with $f_g = 0.733$. They found $H_p = 725$ A/m, $p = 7.3$ and $\langle J_c \rangle = 86$ A/cm^2 which are consistent with the fact that they used a more compact sample having higher f_g.

The fit of the model to the MTG sample data (Fig. 5) was done separately for the two plateaus. We assumed that the grain boundaries are of two different types; one having a very small critical current density J_{c1} that circulates around the grain clusters,[19] and the other with a higher critical current density J_{c2} that circulates around the true grains. The solid lines in Fig. 5 show that the fits are fairly good for the χ' components and poor for the χ'' components. Notice that both fits use $\chi' = -1$ and $\chi'' = 0$ for the maximum magnetic shielding situation at very low fields, $H_m \sim 0.4$ A/m ($\sim$0.005 Oe). Hence, the same scales for χ', χ'', and f_g apply for the whole data independently of the H_m region. This means that the matrix fraction $(1-f_g)$ obtained from the second plateau include the regions between grain clusters as well as between true grains.

The fitting procedure employed for the MTG sample produces only approximate results, mainly due to the arbitrary choice of the data interval, which does not take into account superposition effects caused by the simultaneous occurrence of the different current densities J_{c1} and J_{c2}. In order to minimize the superposition effects we chose the data intervals 0.80 A/m$\leqslant H_m \leqslant$20.0 A/m and 160$\leqslant H_m \leqslant$800 A/m to fit the first and second plateaus, respectively. For the first plateau we found $f_g = 0.994$, $H_p = 8.5$ A/m ($\sim$0.107 Oe), $p = 100$, and $\langle J_{c1} \rangle \approx 1.4$ A/cm^2, while for the second plateau these values are $f_g = 0.931$, $H_p = 334$ A/m ($\sim$4.203 Oe), $p = 0.03$, and $\langle J_{c2} \rangle \approx 54.3$ A/cm^2. Although these values are to be considered as first order approximations, they are however very consistent and corroborate the hypothesis of a multilevel granular structure.[19]

The matrix fraction of about 0.6% associated with bridges of weak superconducting material that separate grain clusters are much smaller than the fraction of about 7% associated with the bridges of stronger superconductivity that separate the tightly joined grains inside the clusters. The average critical current densities $\langle J_{c1} \rangle \approx 1.4$ A/cm^2 and $\langle J_{c2} \rangle \approx 54.3$ A/cm^2 are also consistent with the value of $\langle J_c \rangle \approx 44$ A/cm^2 calculated for the other sintered sample. These values suggest an increasing quality of grain coupling in the following order: (1) poorly joined grain clusters, (2) usual randomly sintered grains, (3) tightly joined oriented grains. The sample quality factor, p, take the values 100, 2.07, and 0.03 in this increasing quality sequence, meaning that *smaller is better*. Possibly this result is connected with the more uniform current distribution throughout the sample matrix when p is smaller, as stated in Eq. (15).

The calculated $\langle J_c \rangle = H_p/a$ is always smaller or, in some cases, equal to a measured transport current, $\langle J_c \rangle_{\text{trans}}$, at zero applied field.[19] This difference is expected to increase with the nonuniformity of the current distribution across the sample, which can be evaluated through the parameter p. Therefore, the calculated values of $\langle J_c \rangle$ for our samples might be taken as underestimated in relation to $\langle J_c \rangle_{\text{trans}}$. The best agreement would be for the tightly joined grains ($p = 0.03$) while the worst would be for the weak grain cluster bridges ($p = 100$).

The occurrence of a third plateau at higher values of H_m, associated with twin boundaries in the MTG sample, is also possible in principle. This would be revealing another type of granularity, in accordance with the general concept of multilevel structure. In this case, much smaller p values and much higher $\langle J_c \rangle$ would be expected, as a consequence of the perfect joining at twin boundaries. An angular dependence of the susceptibility can also be predicted, due to the strong anisotropy involved. However, our homemade susceptometer[24] is limited to a maximum $H_m \approx 1760$ A/m

($\sim$22 Oe), thus preventing the search for the third plateau in the present study. Therefore, this possibility remains as an interesting idea to be tested in the future.

V. CONCLUSIONS

In this paper we discuss the assumptions and the main steps used to derive the average magnetization loops $M(H)$, based on the exponential critical state model for hard type-II superconductors. Two of the expressions derived here for $M(H)$, Eqs. (11) and (12), correct previous results published by Chen *et al.*[17] Using the expressions for $M(H)$ we show how the components of the complex susceptibility can be computed and fitted to the experimental data, with the aid of two free parameters. We have employed this algorithm to analyze the ac susceptibility data obtained for two samples of the high-T_c superconductor $YBa_2Cu_3O_{7-\delta}$. One is a porous sintered sample and the other is a very dense melt-textured sample. The measurements were done by applying only an excitation field whose amplitude varied between 1 and 1760 A/m. Therefore, the data essentially represent a response from the matrix corresponding to the intergranular region of the samples. A clear observation of two plateaus in the component χ' of the susceptibility, associated with a multilevel granular structure in the MTG sample, was possible with our homemade high sensitivity susceptometer. Finally, the calculated components χ' and χ'' furnish fairly good fits of the data for both samples studied.

ACKNOWLEDGMENTS

We thank R. Andrade, Jr. and S. Salem-Sugui, Jr., for providing the samples, and A. C. Lanfredi and A. L. G. Gomes for the computational support. This work was partially supported by Fundação de Amparo a Pesquisa do Estado de São Paulo (Fapesp) and Conselho Nacional de Desenvolvimento Científico e Tecnológico (CNPq).

[1] R. B. Goldfarb, M. Lelenthal, and C. A. Thomson, *Susceptibility of Superconductors and Others Spin Systems*, edited by R. A. Hein, T. L. Francavilla, and D. H. Lieberger (Plenum Press, New York 1991), p. 204.
[2] M. Couach, A. F. Khoder, and F. Monnier, Cryogenics **25**, 695 (1989).
[3] R. B. Goldfarb and A. F. Clark, Cryogenics **27**, 475 (1988).
[4] D. X. Chen and R. B. Goldfarb, J. Appl. Phys. **63**, 980 (1988).
[5] D. C. Larbalestier, S. E. Babcock, X. Cai, M. Daeumling, D. P. Hampshire, T. F. Kelly, L. A. Lavanier, P. J. Lee, and J. Seuntjens, Physica C **153-155**, 1580 (1988).
[6] T. K. Worthington, W. J. Gallagher, and T. R. Dingerm, Phys. Rev. Lett. **59**, 1160 (1987).
[7] S. Tanaka and H. Itozaki, J. Appl. Phys. **27**, L622 (1988).
[8] H. Dersch and G. Blatter, Phys. Rev. B **38**, 11391 (1988).
[9] F. M. A. Moreira, W. A. Ortiz, and O. F. de Lima, Physica C **245**, 3205 (1994).
[10] C. P. Bean, Phys. Rev. Lett. **8**, 250 (1962).
[11] C. P. Bean, Rev. Mod. Phys. **36**, 31 (1964).
[12] H. London, Phys. Lett. **6**, 162 (1963).
[13] Y. B. Kim, C. F. Hempstead, and A. R. Strnad, Phys. Rev. **129**, 528 (1963).
[14] W. A. Fietz, M. R. Beasley, J. Silcox, and W. W. Webb, Phys. Rev. **136**, A335 (1964).
[15] M. Xu, D. Shi, and R. F. Fox, Phys. Rev. B **42**, 10773 (1990).
[16] D. X. Chen and R. B.Goldfarb, J. Appl. Phys. **66**, 2489 (1989).
[17] D. X. Chen, A. Sanchez, and J. S. Muñoz, J. Appl. Phys. **67**, 3430 (1990).
[18] J. L. Chen and T. J. Yang, Physica C **224**, 345 (1994).
[19] D. X. Chen and A. Sanchez, J. Appl. Phys. **70**, 5463 (1991).
[20] T. Ishida and R. B. Goldfarb, Phys. Rev. B **41**, 8937 (1990).
[21] A. Sanchez, Physica C **225**, 136 (1994).
[22] D. Shi, J. G. Chen, S. Salem-Sugui, Jr., and K. C. Goretta, Physica C **185-189**, 2329 (1991).
[23] A. Sanchez and D. X. Chen, *Susceptibility of Superconductors and Others Spin Systems*, edited by R. A. Hein, T. L. Francavilla, and D. H. Lieberger (Plenum, New York, 1991), p. 251.
[24] V. C. Gelfuso and W. A. Ortiz (unpublished).